Chinese Chemical Letters 34 (2023) 107897

Contents lists available at ScienceDirect

Chinese Chemical Letters

journal homepage: www.elsevier.com/locate/cclet

Turning the V site in V@2D-BC_3N_2 complex to high curvature state for efficient CO_2 electroreduction to hydrocarbons

Chaozheng He[a], Yue Yu[a], Chenxu Zhao[a,*], Jinrong Huo[b]

[a] Institute of Environmental and Energy Catalysis, School of Materials Science and Chemical Engineering, Xi'an Technological University, Xi'an 710021, China
[b] School of Sciences, Xi'an Technological University, Xi'an 710021, China

ARTICLE INFO

Article history:
Received 19 September 2022
Revised 5 October 2022
Accepted 12 October 2022
Available online 14 October 2022

Keywords:
V doped 2D BC_3N_2
Curvature effect
CO2 electroreduction
Hydrocarbons production
d-band center theory
Geometric and electronic properties

ABSTRACT

Hydrocarbons are promising products for CO_2 electroreduction (CRR) while is impeded by the low selectivity. Turning the curvature of the active site is an effective strategy to change the adsorption properties and further regulate the product distribution and reactivity. Herein, we have designed a novel V single atom catalyst (SAC) based on rolled two-dimensional (2D) BC_3N_2 substrate with different curvatures. The results have demonstrated that increased curvature can enhance the adsorption strength of CRR intermediates, which follows different mechanisms for systems with low and high curvature. This character eventually leads to the deviation away from the scaling line between E_{ad}[CO]~E_{ad}[COOH] based on transition metals for V@2D-BC_3N_2 systems. 3-3 system is screened as the optimal candidate for hydrocarbons production due to the enhanced binding ability of adsorbates, which can increase the reactivity for hydrocarbons production and hinder the production of H_2 and HCOOH simultaneously.

CO_2 is the ultimate product in the process of utilizing fossil fuels and may cause serious environmental issues like greenhouse effect. It is urgently needed to convert CO_2 into valuable chemicals [1–3]. The electrochemical method is one of the most promising ways [4,5]. The high limiting potential and low selectivity of catalysts are two issues for CO_2 reduction reaction (CRR), and both of them depend strongly on catalysts [6–8]. Although many CRR products possess relatively low equilibrium potentials close to 0 V *vs.* RHE (reversible hydrogen electrode), an acceptable current density of the CRR can only be obtained at around -1.0 V, indicating a large limiting potential caused by the energy loss. Besides, the CRR yields a mixture of different products including CO, hydrocarbons, and HCOOH [9]. Therefore, obtaining high activity for a target reaction product remains a fundamental challenge. Among numerous products of CRR, hydrocarbons, such as CH_4, CH_3OH and C_2H_4, are all valuable chemicals. Cu is found as a unique catalyst that can convert CO_2 into hydrocarbons efficiently in pure transition metals (TMs). However, the large limiting potential of −0.8 V on Cu still hinders its practical application. Thus, it is urgently needed to discover catalysts with high reactivity for CRR to produce hydrocarbons.

In pioneering studies, many works have focused on the single atom catalysts (SAC). As revealed in d-band theory of Norskov, the binding energies of CRR intermediates are strongly correlated with each other on TMs *via* the so-called "scaling relation", which may put a significant limit on the improvement of catalysts [10–12]. SAC is a promising way for breaking the scaling relation and improved reactivity compared to TMs has also been achieved [13,14]. Norskov *et al.* has embedded Pt atom into defective graphene and ultralow limiting potential of -0.27 V is obtained for CRR to CH_3OH [15]. In contrast, Jung *et al.* found that Ir is the favorable dopant for TiC based SAC [16]. The difference of the favorable doped TM atom between Norskov and Jung works can be attributed to the carrier effect. Our previous work has also demonstrated that the two-dimensional (2D) InSe substrate can regulate the metal atoms flexibly to achieve the desired CRR selectivity [17,18]. Besides, the optimal candidates can be screened quickly with the reference of conventional theory on TMs, which is different from the situations in graphene and TiC substrates [15,16,19]. Our results have sufficiently utilized the carrier effect of 2D InSe substrate. To realize quick screen of promising catalysts in a large pool of candidates, we should also make full use of d-band center and descriptors in pioneering studies. Norskov *et al.* have demonstrated that trends in reactivities can be understood in terms of the hybridization energy between the bonding and anti-bonding adsorbate states and the metal d-bands [20]. Moreover, the adsorbate-metal interaction is determined by the filling of the antibonding states on adsorption [21].

* Corresponding author.
E-mail address: zhaochenxu@xatu.edu.cn (C. Zhao).

https://doi.org/10.1016/j.cclet.2022.107897
1001-8417/

Although SAC has been widely investigated in CRR area, the large amounts of candidates still hamper the development of promising catalysts. In pioneering works, Guo *et al.* have also demonstrated that the charge transfer between substrate and metal atoms in SAC plays an important role in promoting the CRR reaction [22]. Curvature effect is one of the most promising ways to regulate the valence of the single metal site, which can reduce the amount of candidates investigated effectively. Sun *et al.* have reported a curvature-dependent selectivity of CRR on Co porphyrin nanotubes (CPN) [23]. The results show that CO is preferred to be produced at low curvature and CH_4 is favored as the curvature increased. Cao *et al.* have compared the curvature effect of Cu and Fe doped carbon nanotubes (Cu@CNT and Fe@CNT) comprehensively [24]. They found that the generation of CO, HCOOH, and CH_3OH is reduced on high-curvature Cu@CNT, which is less notable on Fe@CNT. However, the effect of curvature on the coupling between electric properties, adsorption strength, and reactivity is rather limited in pioneering works, which hinders the development of advanced materials. Referenced to studies of Lei *et al.*, this proposed strategy may benefit from many advatages, including low coordination, lateral heteroatom coordination, and axial heteroatom coordination [25,26].

In our previous work, we have successfully predicted a BC_3N_2 monolayer substrate. This structure is like graphene with B, C and N atoms bonded together upon sp^2 hybridization [27]. Compared with graphene, boron nitride and other graphene materials, each hexagonal primitive unit cell of the BC_3N_2 has one more electron than them. Such a multi-electron system may be beneficial to catalysis due to its advantages in electron transfer rate and effective mass.

Inspired by pioneering and our previous studies, we have herein carried out systematic studies on curvature effect on 2D BC_3N_2 based SAC. About the single atom site, we select V as the dopant in 2D BC_3N_2 due to the unsaturated d orbital (denoted as V@2D-BC_3N_2). This character may contribute to tune the activity and selectivity of CRR *via* curvature. In this work, we have performed density functional theory (DFT) calculations to study CRR on curved V@2D-BC_3N_2 catalyst. Increased curvature can effectively enhance adsorption ability with different mechanism for low- and high- curvature systems. The curvature effect can also regulate the V@2D-BC_3N_2 deviated away from the scaling line between E_{ad}[CO]~E_{ad}[COOH] based on transition metals. 3-3 System (the V@2D-BC_3N_2 systems with 3-3 chirality for 2D BC_3N_2 nanotube) is screened as the optimal candidate for CRR to hydrocarbons, which originates from the enhanced binding ability of CRR intermediates. This character can increase the reactivity of hydrocarbons production and simultaneously hinder the production of H_2 and HCOOH.

All calculations were performed using CASTEP module with the Perdew Burke Erzerhof (PBE) functional [28]. The vacuum thickness was set to be 15 Å to avoid the imaginary interaction between periodic images. The kinetic energy cutoff for plane wave expansions was set to 400 eV and the k points was sampled by Monkhorst-Pack scheme with a grid of $1 \times 2 \times 1$ for all of the 1D nanotubes. The electronic relaxation was performed to within an energy tolerance of 10^{-8} eV for self-consistency, while ionic optimizations were performed until all the residual forces were smaller than 0.005 eV/Å. Electron smearing was employed using the Gaussian-smearing technique with a width of $k_{BT} = 0.1$ eV. Spin-polarized wave functions were used for all calculations. We also include van der Waals (vdW) correction with the MBD method [29,30].

The binding strength of V atom in 2D BC_3N_2 are defined as follows:

$$E_B[\mathrm{V}] = E[\mathrm{V@2D-BC_3N_2}] - E[\mathrm{2D-BC_3N_2}] - E[\mathrm{V}] \quad (1)$$

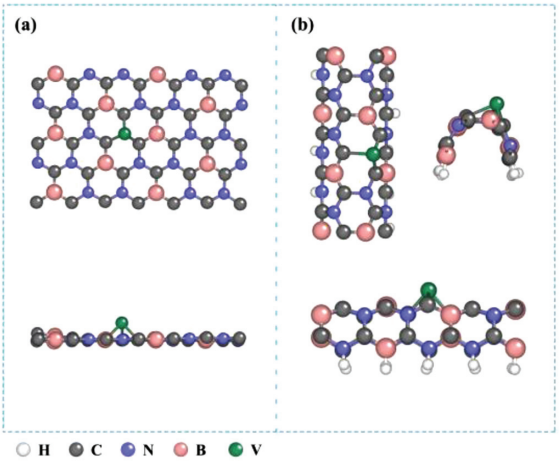

Fig. 1. The top and side view of the (a) pristine and (b) curved V@2D-BC_3N_2.

where E[V@2D-BC_3N_2], E[2D-BC_3N_2] and E[V] denote the electronic energies of V doped 2D BC_3N_2 complex, 2D BC_3N_2 with a vacancy defect, and single V atom. For the coupled proton-electron transfer process, we use the computational hydrogen electrode (CHE) theory [31]. In the CHE scheme, the effect of applied electrode potentials on reaction thermodynamics was based on the free energy change (ΔG_{max}). The relation between the limiting potential (U_L) of the reaction and ΔG_{max} was obtained as $U_L = \Delta G_{max}/e$. Zero point energy and entropy corrections are included for the free energy of adsorbate systems to ensure a fair and unbiased comparison with experiments at 298.15 K.

The change in Gibbs free energy (ΔG) for all electrocatalytic steps was defined as

$$\Delta G = \Delta E + \Delta E_{zpe} - T\Delta S \quad (2)$$

where the reaction energy (ΔE) can be directly determined by analyzing the DFT total energies. ΔE_{zpe} and ΔS are the zero-point energy difference and the entropy difference between the products and the reactants, respectively, and T is the system temperature ($T = 298.15$ K in this work). For each reactant or product, its E_{zpe} value can be calculated by $E_{zpe} = (1/2)\Sigma h\nu$. The entropies of the free molecules were taken from the NIST database, while the energy contribution from the configurational entropy in the adsorbed state is neglected. The solvation effect can be crucial to the CRR, although neither of them is included in the CHE model. However, a model with implicit solvent-electrolyte methods may increase the computational cost by several-fold relative to bias-free modeling [32]. Herein, we mainly focus on screening the optimal catalysts from a large pool of materials and thus take the CHE model as a high-efficiency method.

Partial configurations of the catalysts in the article (Fig. 1) are modelled by the Device Studio program provided by HZWTECH [33].

The above methods have been widely used in pioneering studies especially in catalytic areas [34–48].

The fully relaxed configuration of V@2D-BC_3N_2 is shown in Fig. 1. Two types of nanotubes were constructed denoted as armchair and zigzag types. Each type nanotubes are also constructed with different curvatures. The 2D BC_3N_2 exhibits a hexagonal network structure with one unit cell containing 1B, 2N and 3C atoms. The single V site are located outwards of 2D BC_3N_2 substrate due to the large size of V atom. The curved V@2D-BC_3N_2 appears to show an ellipse shape, which is likely caused by the surface tension. The configurations in Fig. 1a are periodic in the planar directions while it is nanotube structures in Fig. 1b. Thus, we have saturated the edge sites with H atoms.

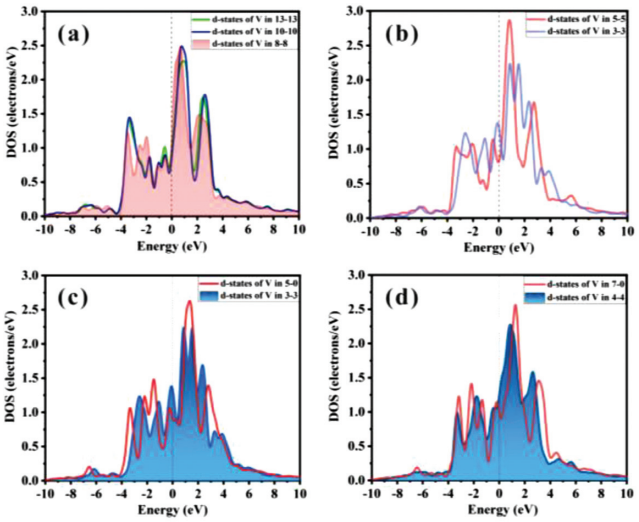

Fig. 2. (a-d) The density of states (DOS) of the d-band for V@2D-BC_3B_2 with different curvature and chiralities.

We first discuss the adsorption sites for V atoms in 2D BC_3N_2. The V atom can replace the B, C and N sites in 2D BC_3N_2. The binding strength of V atom in the N site is generally enhanced compared to other situations (Fig. S1 in Supporting information). We thus select the systems of V doped in N defects as the candidates for this study. The values of binding energies range from −8.8 eV to −9.6 eV referenced to isolated metal atoms in a vacuum. The large values illustrate the thermodynamic stability of our designed catalyst. Referenced to the cohensive energies of V 4-atom (−1.94 eV) and 6-atom (−2.57 eV) cluster [49,50], the binding energies of V in BC_3N_2 nanotubes are significantly larger than the cohensive energies of V clusters. This may indicate that the subsize clusters of V are unlikely to nuclear in our systems. In addition to binding energy, the adsorption energies of *CO and *COOH have exhibited two tendencies for V in N sites: Some candidates comply with the conventional scaling line based on transition metals and others deviate away from the scaling line significantly. In contrast, the adsorption energies of *CO and *COOH for V in B and C sites have totally break the traditional scaling line (Fig. S2 in Supporting information), leading to a difficulty in screening promising catalysts.

In order to clarify the curvature and chirality effect of V@2D-BC_3N_2 nanotubes. We therefore performed density of states (DOS) analysis to investigate the orbital distribution in the bands near Fermi level, which can interact with adsorbates of CRR actively (Fig. 2). As depicted in d-band central theory, the coupling between adsorbate and metal sp state is dominant and constant across different metals. In contrast, the coupling between the adsorbate and metal d state determines the variation of adsorption energy from one metal to the next. In addition, the reactivity of TMs primarily originates from their unsaturated d orbitals. Thus, the comparison of states distribution of V@2D-BC_3N_2 at different curvature is necessary to reveal the electronic properties.

We first discuss the curvature effect in armchair systems. The adsorption energy of CO increases as the curvature increase from 0.12 $Å^{-1}$ (13-13) to 0.50 $Å^{-1}$ (3-3) (Fig. 3 and Table S1 in Supporting information). As shown in Figs. 2a and b, the 10-10 V@2D-BC_3N_2 exhibits increased tendency in the unoccupied states of V d-band above Fermi level compared to 13-13 V@2D-BC_3N_2 and the situation for occupied states is opposite, suggesting that the V atom is positively charged caused by increased curvature. This character indicates that V site can act as an electron-acceptor role and eventually lead to an enhanced adsorption strength for CO. In addition, the 8-8 system demonstrates a wider distribution of

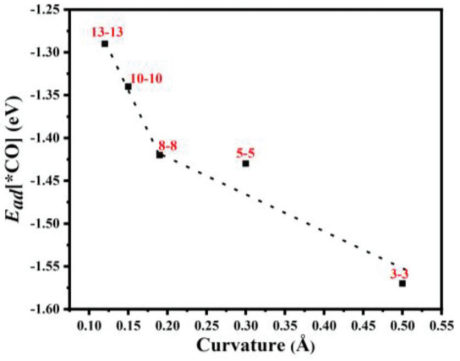

Fig. 3. Correlations between adsorption energies of CO and curvatures.

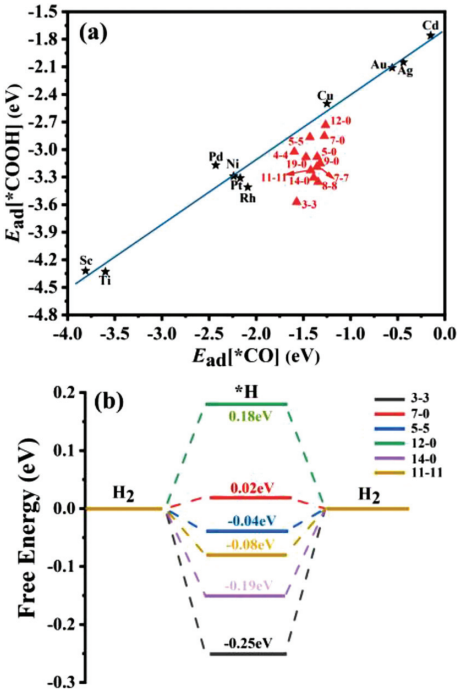

Fig. 4. (a) The correlation between adsorption energies of *CO and *COOH on V@2D-BC_3N_2 (red triangles) and transition metal (111) surfaces (black asterisks). The doping sites of V locate at N vacancies; (b) The hydrogen evolution reaction on different V@2D-BC3N2 nanotubes.

states above Fermi level compared to 10-10. Thus, the ability of gaining electrons is enhanced from 13-13 to 8-8, leading to the increased adsorption ability of V@2D-BC_3N_2. The significant increase of occupied V d-band from 8-8 to 3-3 is beneficial to transfer electrons from V site to adsorbate and eventually contribute to CO adsorption. A change of mechanism has experienced between large and small curvature systems and 8-8 can be treated as the turning point. Thus, the correlation between curvature and adsorption energies can be plotted as two broken lines relation, classified with different adsorption mechanism (Fig. 3). The chirality can also regulate the distribution of V d-states of V@2D-BC_3N_2 with similar curvature (Figs. 2c and d). These characters of the rolled V@2D-BC_3N_2 can be treated as the origin of the flexible regulation for reactivity *via* curvature.

The regulation of curvature can eventually realize the changed adsorption property of CRR intermediates (Fig. S2 and Fig. 4a). The pioneering studies have revealed that binding energies of CRR intermediates correlate with each other *via* scaling relationship due to d-band theory on TMs [11]. However, this relationship will be disturbed on SAC systems. In addition, our previous work has also

demonstrated that the traditional theory of CRR on TMs is still established on SACs that obey the scaling line of TM systems [17]. Referenced to these results, we compare the adsorption energies (E_{ad}) of *CO and *COOH on V@2D-BC_3N_2. Among numerous doping sites of V, N-site systems are particularly interesting. Some systems, such as 4-4, 5-5 and 12-0, comply with the scaling line of TMs and most candidates deviate significantly away from the line. In contrast, the C/N-site systems all possess remarkably high adsorption strength for *CO and *COOH, which may lead to the poisoning effect of active sites. Thus, the N-site systems are the most favorable candidates as CRR catalyst.

It is known that the hydrocarbons production for CRR depends significantly on the binding of *CO and *COOH. We thus analyze the reaction pathway and reactivity based on the adsorption properties in the following part.

The CRR to hydrocarbons on V@2D-BC_3N_2 begins by protonation of CO_2 to carboxyl (*COOH) on the catalysts and *COOH can be further protonated to form *CHO or *COH (Fig. S3 in Supporting information). The formation of *COH is energetically less favorable than *CHO in all cases (Fig. S3 and Table S2 in Supporting information). Additional protonation of *CHO can form either *CH_2OH or *CH_3O. Based on the comparison of free energy change, the minimum energy pathway is generally demonstrated as follows: *$CO_2 \rightarrow$ *COOH $\rightarrow$ *CO $\rightarrow$ *CHO $\rightarrow$ *$CH_2O \rightarrow$ *$OCH_3 \rightarrow$ *O + CH_4. The protonation of *OCH_3 favors the formation of CH_4 compared to CH_3OH, indicating a strong binding ability of *O on V@2D-BC_3N_2. The rate controlling step (RCS) of CRR to hydrocarbon are all *CO $\rightarrow$ *CHO step, except for 3-3 system (*COOH $\rightarrow$ *CO). The change of mechanism in 3-3 system is an interesting phenomenon that should be emphasized (Fig. S4 in Supporting information). This can be interpreted from the general tendency between adsorption energy of *COOH (E_{ad}[*COOH]) and limiting potentials (U_L). For the systems that comply with the scaling line, the limiting potentials are U_L = -0.63 V, -0.5 V, and -0.55 V on 4-4, 5-5, and 12-0 systems, respectively. The values are all favorable than that on Cu (-0.8 V). This may indicate that the change of adsorption energies of *CO/*COOH, complying with the scaling line of TM, can realize the improvement of reactivity. For the systems that disturb the scaling line, the systems exhibit a gradual increased deviation distance from the scaling line in the order of 5-5, 7-0, 11-11, 14-0, 3-3 with the reaction energy (G_r) of *CO $\rightarrow$ *COOH as G_r = 0.5 eV, G_r = 0.44 eV, G_r = 0.33 eV, G_r = 0.29 eV, and G_r = -0.14 eV, respectively. The deviation away from the scaling line of TMs illustrates an enhanced binding strength of *COOH relative to *CO, which may lead to a decreased G_r of RCS (*CO $\rightarrow$ *COOH). Especially for 3-3 system, the *CO $\rightarrow$ *CHO step has become exothermic unlike other systems, which is due to the significant enhancement of *COOH binding with respect to *CO. Besides, the RCS has changed from *CO $\rightarrow$ *CHO to *COOH $\rightarrow$ *CO with an ultralow reaction energy of 0.16 eV, corresponding to a changed mechanism and improved reactivity. This suggests that the curvature effect can indeed change the adsorption properties of CRR intermediates and eventually bring about remarkable reactivity.

About the different regulation level of curvature for *CO and *COOH, it can be interpreted from the adsorption configurations. The *COOH interacts with V@2D-BC_3N_2 bidentate with both C and O atoms while it is monodentate with only C for *CO. This can be treated as the originate for the stabilization of *COOH with respect to *CO.

In addition to hydrocarbons, the production of HCOOH and H_2 are also essential pathways that we cannot ignore. The reaction energies are shown in Fig. 4b and Figs. S5-S7 (Supporting information).

For HCOOH production, the initial protonation of CO_2 can form *HCOO, which can further react to form *HCOOH. The RCSs of HCOOH production are all *HCOO $\rightarrow$ *HCOOH on V@2D-BC_3N_2. We have also calculated the corresponding reaction pathway for the protonation of *HCOOH to *CHO. The RCS for this process is significantly hindered by the *HCOO $\rightarrow$ *HCOOH process with ultrahigh reaction energies of 0.87$\sim$1.15 eV (Figs. S5-S7). Thus, *CHO can only be produced *via* *COOH intermediate. The limiting potential of HCOOH production on 3-3 system is -1.92 eV, indicating that HCOOH can be effectively hindered *via* curvature regulation. Compared with other systems like 12-0 system, the adsorption energy of *HCOO (*HCOOH) is enhanced from -0.99 (-0.89) eV to -1.43 (-1.08) eV. The value has increased 0.44 eV for *HCOO and it is only 0.19 for *HCOOH, indicating that *HCOO is considerably stabilized with respect to *HCOOH at high curvature state. This can be treated as the origin of high selectivity for hydrocarbons compared to HCOOH on 3-3 system.

Similar conclusion can also be found for H_2 production. The hydrogen adsorption free energy (ΔG_H) is always treated as the measurement of reactivity. As the systems deviate away from the scaling line of TMs in the order of 12-0, 7-0, 11-11, 14-0, 3-3, the ΔG_H exhibits a negative shift tendency (0.18, 0.02, -0.08, -0.15 and -0.25 eV for 12-0, 11-11, 14-0 and 3-3, respectively) and eventually leads to a high limiting potential of -0.25 V on 3-3. Thus, CRR is more preferred on 3-3 than HER and the opposite regulation tendency between curvature and reactivity is particularly interesting.

Above all, the high-curvature states may lead to enhanced binding ability for CRR/HER intermediates. This is beneficial for hydrocarbons production and unfavorable for H_2 and HCOOH production.

In this work, we have performed density functional theory calculations to study CRR to hydrocarbons on curved V@2D-BC_3N_2 catalyst. Curvature can effectively enhance adsorption ability with different mechanism. For low (high) curvature systems, the unoccupied (occupied) d-states are increased with increasing curvature and V acts as the electron acceptor (donor). 8-8 system is the tuning point with wider distributed d-states. The curvature effect can also regulate the V@2D-BC_3N_2 systems with different deviation distance from the scaling line between E_{ad}[CO]$\sim$$E_{ad}$[COOH] based on transition metals. The high curvature state (3-3 system) can induce high binding ability for CRR intermediates, which can induce increased (decreased) reactivity for hydrocarbons (HCOOH and H_2) production. Thus, 3-3 system is screened as the optimal candidate for CRR to hydrocarbons with different rate controlling step of *COOH $\rightarrow$ *CO compared to other systems (*CO $\rightarrow$ *CHO), which is due to the stabilization of *COOH with respect to *CO.

Declaration of competing interest

The authors declare that they have no known competing financial interests or personal relationships that could have appeared to influence the work reported in this paper.

Acknowledgments

This work was supported by the National Natural Science Foundation of China (No. 21603109), the Henan Joint Fund of the National Natural Science Foundation of China (No. U1404216), the Special Fund of Tianshui Normal University, China (No. CXJ2020-08) and the Scientific Research Program Funded by Shaanxi Provincial Education Department (No. 20JK0676). This work was also supported by Natural Science Basic Research Program of Shanxi (Nos. 2022JQ-108, 2022JQ-096). In addition, this work was also partially supported by the Postgraduate Research Opportunities Program of HZWTECH (No. HZWTECH-PROP).

Supplementary materials

Supplementary material associated with this article can be found, in the online version, at doi:10.1016/j.cclet.2022.107897.

References

[1] B. Yang, L. Li, L. Guo, et al., Chin. Chem. Lett. 31 (2020) 2627–2633.
[2] S. Gong, G. Zhu, M. Hojamberdiev, et al., Appl. Catal. B: Environ. 297 (2021) 120413.
[3] L. Wang, G. Huang, Q. Wang, et al., J. Energy Chem. 64 (2022) 85–92.
[4] M. Aresta, A. Dibenedetto, A. Angelini, et al., Chem. Rev. 114 (2014) 1709–1742.
[5] D.T. Whipple, P.J.A. Kenis, J. Phys. Chem. Lett. 1 (2010) 3451–3458.
[6] K.P. Kuhl, T. Hatsukade, T.F. Jaramillo, J. Am. Chem. Soc. 136 (2014) 14107–14113.
[7] K.P. Kuhl, E.R. Cave, T.F. Jaramillo, et al., Energy Environ. Sci. 5 (2012) 7050–7059.
[8] X. Fu, H. Yang, L. Li, et al., Chin. Chem. Lett. 32 (2021) 1089–1094.
[9] R. Kortlever, J. Shen, M.T.M. Koper, et al., J. Phys. Chem. Lett. 6 (2015) 4073–4082.
[10] H. Shin, Y. Ha, H. Kim, J. Phys. Chem. Lett. 7 (2016) 4124–4129.
[11] A.A. Peterson, J.K. Norskov, J. Phys. Chem. Lett. 3 (2012) 251–258.
[12] F. Abild-Pedersen, J. Greeley, J.K. Norskov, et al., Phys. Rev. Lett. 99 (2007) 016105.
[13] B.T. Qiao, A.Q. Wang, T. Zhang, et al., Nat. Chem. 3 (2011) 634–641.
[14] Z.W. Huang, X. Gu, X.F. Tang, et al., Angew. Chem. Int. Ed. 51 (2012) 4198–4203.
[15] C. Kirk, L.D.C. Section, J.K. Norskov, ACS Central Sci. 3 (2017) 1286–1293.
[16] S. Backs, Y.S. Jung, ACS Energy Lett. 2 (2017) 969–975.
[17] C.X. Zhao, G.X. Zhang, W. Gao, Q. Jiang, J. Mater. Chem. A 7 (2019) 8210–8217.
[18] C. Zhao, M. Xi, J. Huo, C. He, Phys. Chem. Chem. Phys. 23 (2021) 23219–23224.
[19] S. Back, J. Lim, N.Y. Kim, Y.H. Kim, Y. Jung, Chem. Sci. 8 (2017) 1090–1096.
[20] B. Hammer, J.K. Norskov, Surf. Sci. 343 (1995) 211–220.
[21] B. Hammer, J.K. Norskov, Nature 376 (1995) 238–240.
[22] X. Wang, H. Niu, Y. Guo, et al., Catal. Sci. Technol. 10 (2020) 8465–8472.
[23] G.Z. Zhu, Y.W. Li, Q. Sun, et al., ACS Catal 6 (2016) 6294–6301.
[24] Y. Zhang, L. Fang, Z. Cao, RSC Adv 10 (2020) 43075–43084.
[25] Y.C. Wang, Q.C. Wang, Y.P. Lei, et al., Nano Energy 103 (2022) 107815.
[26] Q.C. Wang, Y.C. Wang, Y.P. Lei, et al., Nat. Commun. 13 (2022) 3689.
[27] J. Yu, C. He, L. Yu, et al., Chin. Chem. Lett. 32 (2021) 3149–3154.
[28] M.D. Segall, P.J.D. Lindan, M.C. Payne, et al., J. Phys. Condens. Matter. 14 (2002) 2717–2744.
[29] A. Tkatchenko, M. Scheffler, Phys. Rev. Lett. 102 (2009) 073005.
[30] N. Marom, A. Tkatchenko, L. Kronik, et al., J. Chem. Theory Compt. 7 (2011) 3944–3951.
[31] J.K. Norskov, J. Rossmeisl, H. Jonsson, et al., J. Phys. Chem. B 108 (2004) 17886–17892.
[32] J.A. Gauthier, S. Ringer, J.K. Norskov, et al., ACS Catal 9 (2019) 920–931.
[33] Hongzhiwei Technology, Device Studio, Version 2021A, China, Available online 2021, http://iresearch.net.cn/cloudSoftware (accessed on 2021/08/01).
[34] C. Li, D. Lu, C. Wu, J. Indust. Engin. Chem. 98 (2021) 161–167.
[35] Y. Linghu, D. Lu, C. Wu, J. Phys. Condens. Matter. 33 (2021) 165002.
[36] Y. Liu, Q. Feng, Y. Lei, et al., Nano Energy 81 (2021) 105641.
[37] H. Peng, J. Ren, Y. Lei, et al., Nano Energy 88 (2021) 106307.
[38] F. Rao, G. Zhu, M. Hojamberdiev, et al., Appl. Catal. B: Environ. 281 (2021) 119481.
[39] F. Rao, G. Zhu, M. Hojamberdiev, et al., ACS Catal 11 (2021) 7735–7749.
[40] L. Wang, X. Shi, Q. Wang, et al., Chin. Chem. Lett. 32 (2021) 1869–1878.
[41] S. Zhang, D. Chen, Z. Liu, et al., Appl. Catal. B: Environ. 284 (2021) 119686.
[42] S. Zhang, B. Zhang, Z. Liu, et al., Nano Energy 79 (2021) 105485.
[43] S. Zhou, K. Chen, Q. Wang, et al., Appl. Catal. B: Environ. 266 (2020) 118513.
[44] J. Chen, H. Lei, X. Dong, et al., J. Colloid Interface Sci. 601 (2021) 704–713.
[45] R. Guo, K. Zhang, M. Jin, et al., J. Mater. Chem. A 9 (2021) 6196–6204.
[46] X. He, M. Wu, S. Wang, et al., J. Hazard Mater. 403 (2021) 124048.
[47] H. Lei, M. Wu, X. Dong, et al., Chin. Chem. Lett. 32 (2021) 2317–2321.
[48] H. Lei, M. Wu, Z. Wu, et al., Environ. Sci. Nano 8 (2021) 1398–1407.
[49] S.E. Weber, B.K. Rao, P.H. Dederichs, et al., J. Phys. 9 (1997) 10739–10748.
[50] X.Y. Wu, A.K. Ray, J. Chem. Phy. 110 (1999) 2437–2445.